Desalination 517 (2021) 115244

Contents lists available at ScienceDirect

Desalination

journal homepage: www.elsevier.com/locate/desal

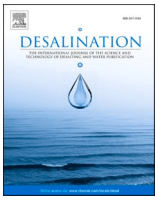

Field synergy analysis for heat and mass transfer characteristics in adsorption-based desalination and cooling systems

Mingliang Li, Yanan Zhao, Rui Long *, Zhichun Liu, Wei Liu

School of Energy and Power Engineering, Huazhong University of Science and Technology, Wuhan 430074, PR China

HIGHLIGHTS

- Field synergy analysis is conducted to illustrate the heat and mass transfer characteristics in the adsorption process
- Two field synergy angles reflecting the synergy effect of heat transfer and flow resistance are proposed
- Impacts of bed configurations are explored under the guidance of field synergy analysis
- The SCP and SDWP in the fork-row arrangement are 6.6% higher than those in the in-line arrangement

ARTICLE INFO

Keywords:
Adsorption desalination
Heat and mass transfer
Field synergy
CFD model
Finned-flat bed

ABSTRACT

Adsorption-based desalination and cooling system has gained particular interests for low-grade heat harvesting. In this study, field synergy analysis is conducted to illustrate the complicated heat and mass transfer characteristics in an adsorption-based desalination and cooling system with finned-flat beds via a dynamical three-dimensional computational fluid dynamics model. Two field synergy angles α and β reflecting the synergy effect of heat transfer and flow resistance with the adsorption driving force are examined. Results illustrate that smaller α and β result in better adsorption performance. Furthermore, guided by the field synergy analysis, adsorbent bed configurations (fin diameter, fin pitch, fin shape, and fin arrangement) are optimized. The fork-row arrangement results in a higher SCP and SDWP than that of the in-line arrangement. With the fin pitch of 20 mm and fin diameter of 12 mm, the system with fork-row arrangement demonstrates a SCP of 0.363 kW/kg and SDWP of 12.5 m^3 per ton silica gel per day, which is 6.6% higher than that of the in-line arrangement as the field synergy parameter between heat transfer and the driving force factor (α) is more predominant at a relatively smaller fin pitch.

1. Introduction

Cooling and fresh water are two main necessities of human's life continuation, especially in Gulf regions with water scarcity under tropical desert climate, and a lot of energy-intensive factories are built to meet the demands of cooling and potable water [1–3]. The combustion of fossil fuel has induced a series of environmental problems, such as harmful emissions and the notorious greenhouse effect. Conventional vapor compression cooling system is limited as it consumes a large amount of electricity and causes ozone depletion with the wide utilization of hydrochlorofluorocarbons (HCFCs) [4,5]. In recent years, efforts have been devoted to adsorption-based desalination and cooling systems, which simultaneously provide cooling load as well as fresh water driven by low-grade heat [6–8]. The adsorption-based system has the advantages of low energy consumption and using environmentally friendly refrigerant such as water, benefiting for the global warming and ozone depletion [9–12]. In addition, as pressure lift is conducted via the thermal process, the adsorption-based system has many other advantages such as low operating costs, few moving parts, simple control and vibration-free operation [13]. However, the low thermal conductivity and mass transfer efficiency [14], making the system a low specific cooling power and large volume that hinder the wide commercialization of adsorption-based systems.

Studies have been carried out to conquer the drawbacks of adsorption-based systems, which can be classified as: (i) investigation of novel or composite adsorbents [15] with favorable adsorption kinetics, such as the metal organic frame work (MOF) [16–18], a high hydrophilic

* Corresponding author.
E-mail address: r_long@hust.edu.cn (R. Long).

https://doi.org/10.1016/j.desal.2021.115244
Received 2 April 2021; Received in revised form 17 June 2021; Accepted 11 July 2021
Available online 24 July 2021

Nomenclature

C_p	Specific heat, J kg^{-1} K^{-1}
COP	Coefficient of performance, –
d_p	Particle diameter, m
D_s	Mass diffusivity, m^2 s^{-1}
D_{so}	Pre-exponential factor, m^2 s^{-1}
E	Characteristic energy, J mol^{-1}
E_a	Activation energy, J mol^{-1}
H_a	Heat of adsorption, J kg^{-1}
h_{fg}	Latent heat of vaporization, J kg^{-1}
h	Convective heat transfer coefficient, W m^{-2} K^{-1}
K	Permeability, m^2
k	Thermal conductivity, W m^{-1} K^{-1}
M, m	Mass, kg
Nu	Nusselt number, –
n	Surface heterogeneity factor of the adsorption materials, –
P	Pressure of adsorption/desorption, Pa
P_s	Saturation pressure, Pa
Q	Heat, J
Q_{st}	Isosteric heat of adsorption, kJ kg^{-1}
R	Universal gas constant, J mol^{-1} K^{-1}
SCP	Specific cooling power, kW/kg
SDWP	Specific daily water production, m^{-3} ton^{-1} day^{-1}
T	Temperature, K
TCP	Total cooling power, kW
t	Time, s
U	Velocity vector, m s^{-1}
W	Water uptake, kg kg^{-1}
W_∞	Maximum adsorbent capacity, kg kg^{-1}
W_o	Equilibrium uptake, kg kg^{-1}

Greek symbols

ε	Porosity, –
μ	Dynamic viscosity, Pa s
ρ	Density, kg m^{-3}
α	Thermal diffusivity, m^2 s^{-1}

Subscripts

ads	Adsorption
b	Bed
c	Cooling, condenser
con	Condenser
des	Desorption
eva	Evaporation
e	Evaporator
f	Fluid
g	Gas phase
i	Initial
m	Metal
p	Particle
sat	saturation
s	Solid phase, saturated, saline
t	Total
v	Vapor phase
w	Water

material which has gained significant interest in adsorption study in the last few decades, and SWS-1 L [19], a silica gel adsorbent which is commixed with $LiNO_3$ to enhance its hydrophilicity; (ii) system and cycle optimization to decrease the pressure lift, for instance, multi-bed and multi-stage adsorption system [20–22] or heat recovery [23–25] between the evaporator and condenser; (iii) optimization of the heat exchanger [26] to promote the discharge of adsorption heat or investigation of the optimal operation conditions comprising of cycle time, heating temperature, evaporator pressure etc. [27,28]; (iv) grain level studies to investigate the adsorption dynamics and the mono or multi-layer adsorption mechanism [29–31]. Among the simulation literature, there are two models which are the most popular [32]: the lumped model (LP) and the computational fluid dynamic (CFD) model. The former is based on differential-algebraic systems to solve the heat transfer problem, while the latter addresses the heat and mass transfer with partial differential equations. LP model has a basic assumption that the bed is near isobaric and isothermal, which makes it less computational demanding and relatively low accuracy, while the CFD model considers the temperature and pressure jump thus the heat and mass transfer mechanisms. The CFD model can be classified into three types: isobaric temperature jump method [33], isothermal pressure jump method [34], the non-isothermal and non-isobaric method [35]. Despite intensive computational requirement, the CFD model is essential to simulate adsorption kinetics inside a practical adsorber. The numerical result derived from the lumped model may have a large deviation with the experimental data and the CFD results, as it neglects the temperature and pressure variation within the bed, which is significant in some situations [36].

As shown in Fig. 1, the adsorption reaction is predominantly manipulated by three processes [37]: (i) inter-particle mass transfer resistance while the vapor flows through the torturous void space between adsorbent grains, which macroscopically manifests as the pressure drop along the vapor flow path; (ii) intra-particle diffusion resistance arising due to the inherent micro-pore inside the adsorbent

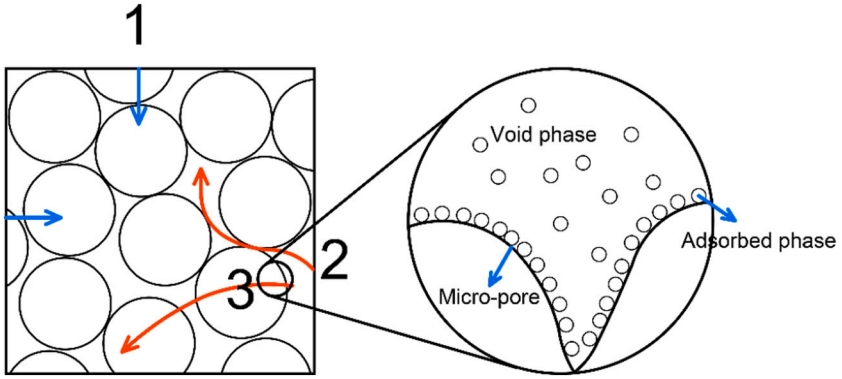

Fig. 1. Three significant processes in the adsorption. 1: heat transfer; 2: inter-particle permeation; 3: intra-particle diffusion.

grain, which is demonstrated as the predominant decisive step of the adsorption reaction (i.e. the adsorption kinetic); (iii) heat transfer within the bed to liberate the adsorption heat, which is eventually taken away by the cold fluid. Inserting metal fins in the bed can effectively enhance heat exchange between the adsorbent and cold fluid, thus facilitating the release of adsorption heat. These three processes are corresponding to heat transfer, mass transfer, and flow resistance respectively, which are the most important factors in an adsorption bed. Saleh et al. [38] compared the performance of an adsorption heat pump utilizing the wire fin heat exchanger with rectangular finned and microchannel finned bed. The results presented that pressure drop inside a microchannel heat exchanger is approximately 5 times larger than the other two finned beds, denoting its fairly high flow resistance. With a larger heat exchange surface between aluminum fumarate particles and the cold source, the wire finned bed shown superior performance in terms of bed temperature and water uptake. Niazmand et al. [39] established a transient two-dimensional CFD model to examine the performance of a cylindrical bed with annular fins using silica gel/water pair. Bed configurations comprising of fin spacing, bed height and grain diameter are examined to explore their effects on performance parameters such as specific cooling power (SCP), total cooling power (TCP) and coefficient of performance (COP). The simulation results presented a viable method to dramatically reduce the bed volume at the cost of slightly reducing COP. Kowsari et al. [40] developed a three-dimensional numerical model to examine the effect of bed configurations such as fin pitch and fin height on the system performance in terms of cycle time, SCP and COP. Their study considered a finned-flat tube heat exchanger, for which the rectangular and the corresponding trapezoidal fins are compared. With a systematic bed designing procedure for performed parametric conditions proposed, this type of heat exchanger can be designed more effectively and appropriately for adsorption utilization.

Among the three significant factors manipulating the adsorption process, heat conduction is the most predominant in many conditions, as the grain diameter impacting the adsorption kinetics is normally invariant and the effect of flow resistance can be neglected in many cases. Nevertheless, via an order of magnitude analysis of the continuity, momentum and energy equations, Mitra et al. [37] found that there is a critical value for the bed aspect ratio beyond which the flow resistance and pressure drop become significant instantaneously. Subsequently, they examined the effect of particle diameter and aspect ratio on the adsorption dynamics with a two-dimensional CFD model [36]. Li et al. [41] conducted a comprehensive analysis about the effect of stepwise porosity distributions inside a finned-tube bed on system performance of adsorption-based desalination and cooling system via transient CFD model, and found that the forward distributions presents obviously augmented cooling as well as water production.

In adsorption-based desalination and cooling systems, the flow resistance, adsorption kinetics and heat transfer impact the adsorption process simultaneously and directionally, which are often illustrated separately. In this study, field synergy analysis is conducted to illustrate the complicated heat and mass transfer characteristics in an adsorption-based desalination and cooling system with finned-flat beds via a dynamical three-dimensional computational fluid dynamics model. Two field synergy angles α and β reflecting the synergy effect of heat transfer and flow resistance with the adsorption driving force are examined. In addition, guided by the field synergy analysis, adsorbent bed configurations (fin diameter, fin pitch, fin shape, and fin arrangement) are optimized, and some useful conclusions are drawn.

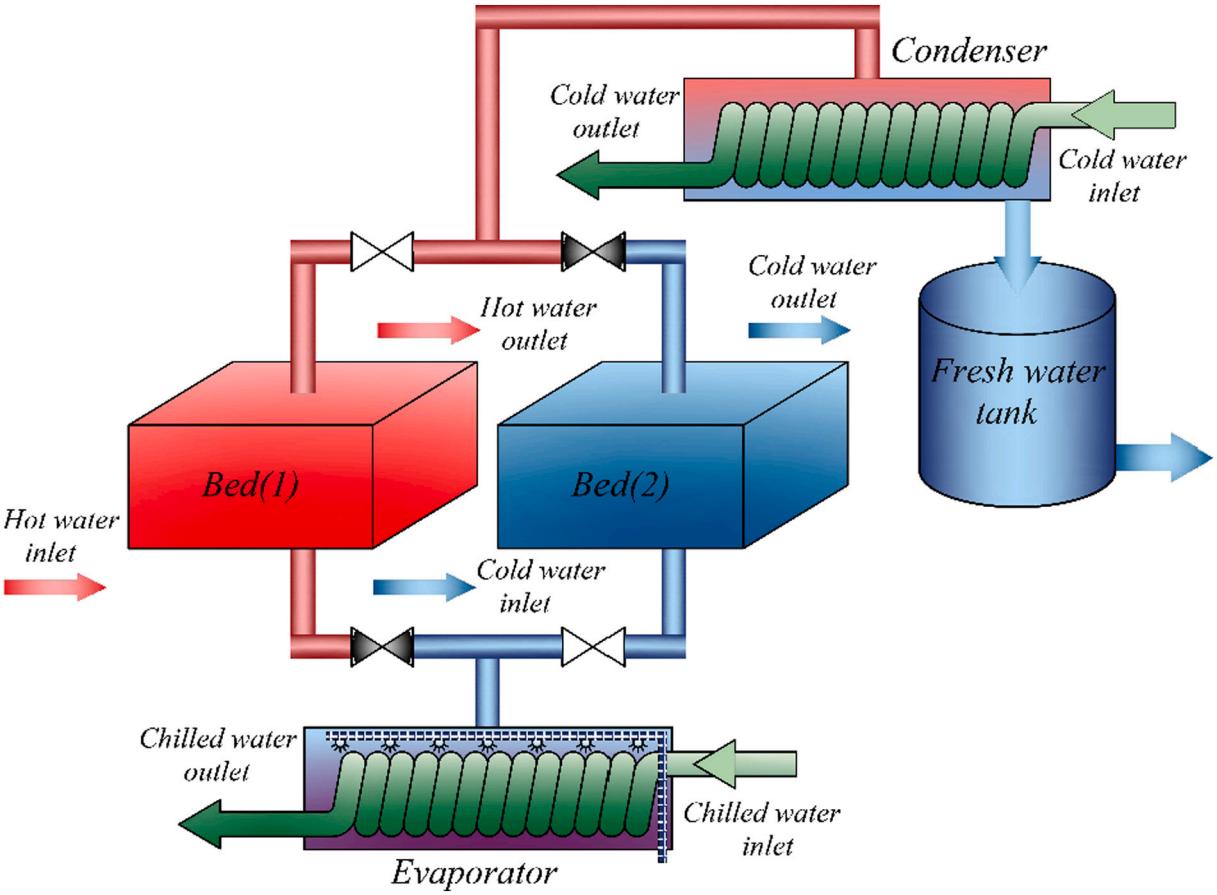

Fig. 2. Schematic of the simulated adsorption cooling and desalination system.

2. Physical model

2.1. Description of the physical model

As presented in Fig. 2, the model utilized in this study considers a whole adsorption cooling and desalination cycle comprising four steps: adsorption, preheating, desorption and precooling. During the adsorption process, the bed is communicated with an evaporator while sea water vaporizes under the effect of adsorbent particles. Simultaneously the coolant flows through to take away adsorption heat. Then the bed is preheated until its pressure elevates to the condenser pressure. The vapor is regenerated and fresh water is produced in the condenser. Finally, the bed is precooled and the next cycle is ready to begin. It has been demonstrated in our prior study that the system comes to a cyclic steady state after 4–5 cycles. All the physical parameters are derived from the adsorption process after the cycle stabilizes. The simulated finned-flat bed is presented in Fig. 3A. The modular bed advanced by Mohammed [42] is inserted by many columnar fins which can further strengthen the bed heat exchange with coolant or hot water. Loose silica gel grains are packed on an aluminum plate with many cylindrical fins standing upright, with cold or hot water flows below, and vapor enters from the top. Two different fin arrangements, in-line and fork-row (i.e. square arrangement and triangular arrangement), are presented in Fig. 3B and C. The particular bed geometric parameters are listed in Table 1. The detailed scheme of dimensions is presented in Table 2.

In order to save the computational cost, several assumptions and simplifications are developed based on prior literature [43]:

1. The diameter of adsorbent grains is invariant.
2. The vapor phase is an ideal gas phase.
3. Pressure drop inside the bed can be described according to Darcy's law.

Table 1
The bed geometric and model parameters.

h(mm)	T_{eva}(°C)	T_{con}(°C)	T_{hw}(°C)	T_{cw}(°C)	h(W/m^2·K)
12	15	25	85	25	500

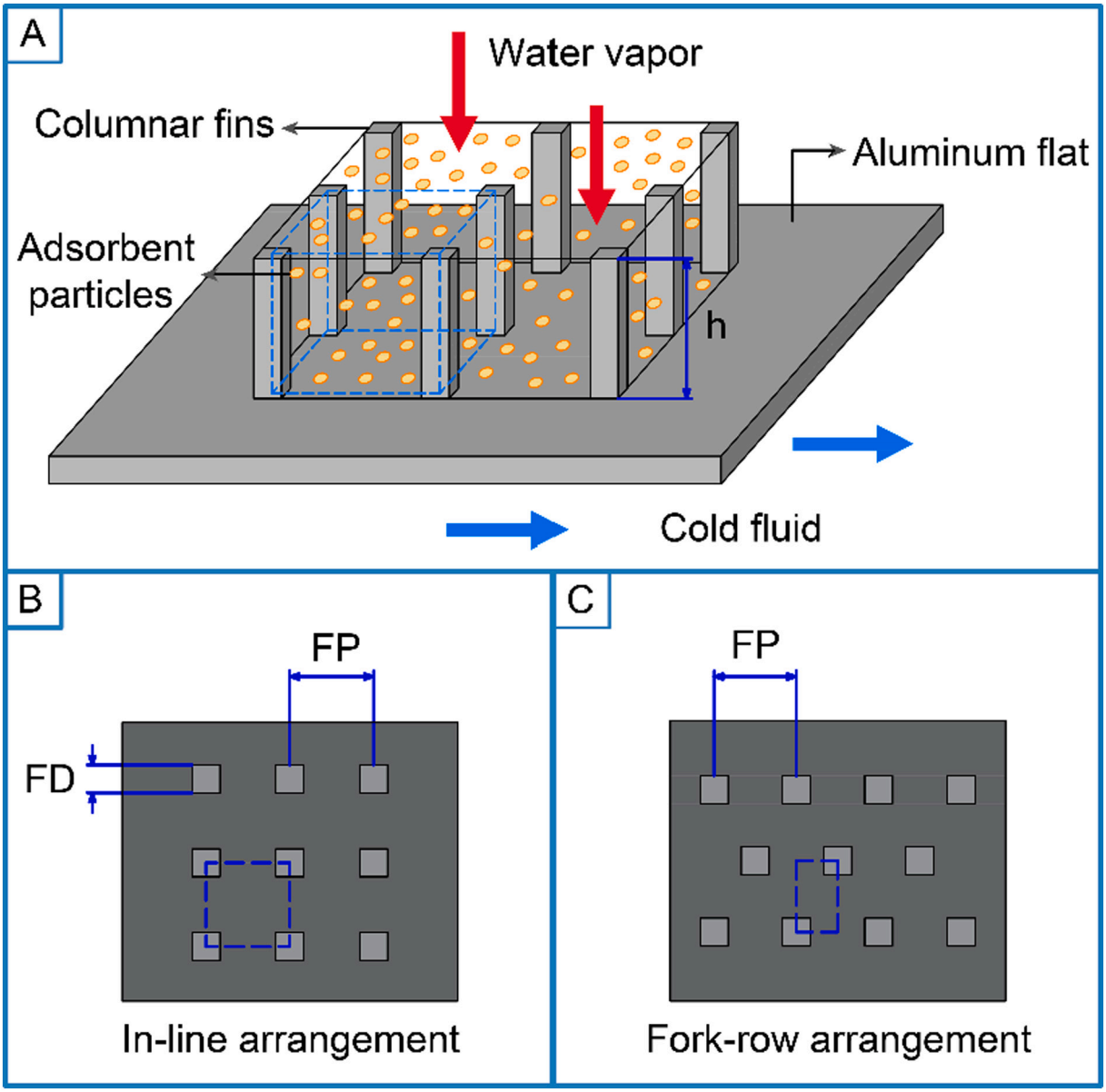

Fig. 3. Schematic of the simulated finned-flat bed (A) and the in-line arrangement (B), fork-row arrangement (C).

Table 2
The scheme of dimensions.

Fin pitch (mm)	Fin diameter (mm)	Fin shape
5	0.5, 1, 1.5, 2, 2.5, 3	Rectangular, rhombus, circle
10	1, 2, 2.5, 3, 3.5, 4, 4.5, 5, 6	
20	2, 3, 4, 5, 6, 8, 10, 12	

4. Thermal conductivity, specific heat capacity and viscosity are independent of temperature.
5. The contact thermal resistance at all phase interfaces can be neglected.
6. Temperatures of the cold and hot water are constant during each step.
7. The convective heat transfer resistance is invariant and reasonably selected from Ref. [44].

2.2. Governing equations

During the adsorption process, flow resistance, adsorption kinetic and heat transfer are the three significant factors among which flow resistance arouses vapor pressure drop along the flow path. As the inertial term and viscosity term in the momentum equation can be neglected compared with Darcy's term, the inter-grain mass transfer resistance can be described using Darcy's law:

$$\overrightarrow{U} = -\frac{K}{\mu}\nabla P \tag{1}$$

where μ is the water vapor viscosity, $\overrightarrow{U}$ is the vapor velocity vector, K the bed permeability, which can be derived using the Blake-Kozeny equation.

$$K = \frac{d_p^2 \varepsilon_b^3}{150(1-\varepsilon_b)^2} \tag{2}$$

where d_p is the adsorbent grain diameter, ε_b the bed porosity. It should be noted that ∇P is the pressure gradient. As augmenting the flow resistance leads to a larger pressure drop, in the subsequent synergy analysis, this parameter is selected as a significant value to directly reflect the inter-particle mass transfer resistance.

The adsorption dynamic characteristic is captured using the linear driving force (LDF) model [45], via which the inter-particle mass diffusion resistance is reflected.

$$\frac{\partial W}{\partial t} = \frac{60 D_s}{d_p^2}(W_o - W) \tag{3}$$

where W is the instantaneous uptake, W_o the equilibrium uptake, D_s the surface diffusivity which can be calculated by:

$$D_s = D_{so} exp\left(-\frac{E_a}{RT_s}\right) \tag{4}$$

where D_{so} is the pre-exponential factor, E_a the activation energy, T_s the adsorbent temperature.

The equilibrium uptake can be captured via the D-A equation [46].

$$X_o = X_\infty exp\left(-\left(\frac{RT_s}{E} ln\left(\frac{P_s}{P}\right)\right)^n\right) \tag{5}$$

where X_∞ is the maximum uptake of silica gel, E the characteristic energy, R the universal gas constant, n the heterogeneity factor, P the vapor pressure, and P_s the saturated pressure of water vapor at the bed temperature. All the thermophysical parameters used in the modeling are listed in Table 3.

The term $(\frac{\partial W}{\partial t})$ in LDF represents the rate of adsorption reaction, while the right term $(W_o - W)$ represents the distance to reach adsorption equilibrium, or the reaction imbalance. Evidently, a larger distance to obtain equilibrium $(W_o - W)$ accelerates the adsorption rate, thus it can be regarded as the driving force of reaction and used in the field synergy analysis.

The adsorption process should fit the energy conservation equation [48]:

$$\left(\varepsilon_b \rho_v C_{pv} + \rho_b C_{ps} + \rho_b X C_{pw}\right)\frac{\partial T_v}{\partial t} + \rho_v C_{pv}\overrightarrow{U}\cdot\nabla T = \nabla\cdot\left(k_{eff}\nabla T\right) + \rho_b H_\alpha \frac{\partial X}{\partial t} \tag{6}$$

where C_{ps} is the specific heat capacity of adsorbent, H_a the isosteric adsorption heat. The first term on the left is the non-steady-state term, representing variations in internal energy over time. The two terms on the right side of the equation are the conduction term and the source term, respectively, while the second term on the left is the convection term which is neglectable compared with the conduction term. It should be emphasized that ∇T is the temperature gradient that represents the heat transfer factor in accordance with Fourier Law. Further analysis on this parameter will be conducted in the field synergy description.

The heat conduction inside the aluminum flat and fin can be described by [49,50]:

$$\frac{\partial T}{\partial t} = \alpha \nabla^2 T \tag{7}$$

where α is the thermal diffusivity of aluminum.

Apart from the aforementioned momentum equation, dynamic equation and energy equation, the fluid should also fit the continuity equation [51,52]:

$$\frac{\partial(\varepsilon_t \rho_v)}{\partial t} + \nabla\cdot\left(\rho_v \overrightarrow{U}\right) + \rho_b \frac{\partial X}{\partial t} = 0 \tag{8}$$

where ρ_v is the vapor density, ρ_b the bed density, $\overrightarrow{U}$ can be obtained from Darcy's law, ε_t is the total porosity which can be calculated by the particle porosity ε_p and bed porosity ε_b: $\varepsilon_t = \varepsilon_b + \varepsilon_p(1-\varepsilon_b)$. The three terms on the left are the unsteady term, the velocity term and the mass source term, respectively.

2.3. Boundary conditions and model validation

As shown in Table 1, the coolant, condenser and heating temperatures are fixed at 25 °C, 25 °C and 85 °C, which is appropriate in a low-

Table 4
Initial and boundary conditions.

Initial conditions	
$P=P_{sat}@T_{eva}$; $X = X_0@(T = 60\ °C, P=P_{eva})$; $T = T_{cw}$; $M_{sw} = M_0$	
Boundary conditions	
Preheating process	$T_f = T_{hw}$
Desorption process	$T_f = T_{hw}$; $P(H) = P_{con}$
Precooling process	$T_f = T_{cw}$
Absorption process	$T_f = T_{hw}$; $P(H) = P_{eva}$

Table 3
The thermophysical parameters of silica gel [47].

$C_{ps}\left(\frac{kJ}{kg\cdot K}\right)$	$E_a\left(\frac{J}{mol\cdot K}\right)$	$D_{so}\left(\frac{m^2}{s}\right)$	$\rho_b\left(\frac{kg}{m^3}\right)$	$d_p(mm)$	$k_b\left(\frac{W}{m\cdot K}\right)$	$H_a\left(\frac{kJ}{kg}\right)$	$X_\infty\left(\frac{kg_v}{kg_a}\right)$	$E\left(\frac{J}{mol}\right)$	n
924	42,000	2.54×10^{-4}	740	0.35	0.198	2415	0.37	4280	1.15

grade heat driving adsorption system. All the initial and boundary parameters have been listed step by step in Table 4. In order to simplify the calculation, the coolant and hot water flow is not simulated with the convective heat transfer coefficient of 500 W/m^2·K [44]. In the simulation, the evaporator temperature is set at 15 °C, and the evaporator pressure (P_{eva}) is calculated via a time-dependent equation:

$$P_{eva} = (1 - 0.537S)P_{sat} \tag{9}$$

where $P_{sat} = 8.143 \times 10^{10} \exp(-5071.7/T)$ is the saturation pressure at temperature T. S is the salinity [53] which can be captured using the initial concentration of sea water and the variation rate of adsorption uptake ($\frac{\partial W}{\partial t}$). The model is well validated via a comparison of numerical results with the experimental and simulated data obtained from literature. The details of model validation and the boundary conditions including each step of the cycle can be found in our previous study [41].

All the geometrical parameters are presented in Table 1. The total bed module is fixed at 20 mm × 20 mm with a bed height of 12 mm. The governing equations are well solved using COMSOL Multiphysics 5.5 with a mesh size of 4662.

2.4. Field synergy analysis

Although the uptake and SCP are directly manipulated by the adsorption kinetics, the synergistic effect of heat transfer as well as flow resistance on the adsorption dynamics is significant. In order to explore the synergy effect between them, three physical quantities that can intuitively reflect the three processes are essential. Based on the analysis of governing equations, three significant factors (∇P, $W_o - W$, ∇T) are selected to reflect flow, reaction and heat transfer driving force. In addition, two synergy angles are proposed:

$$\alpha = arccos\frac{\nabla T \cdot \nabla(W_o - W)}{|\nabla T| \cdot |\nabla(W_o - W)|} \tag{10}$$

$$\beta = arccos\frac{\nabla P \cdot \nabla(W_o - W)}{|\nabla P| \cdot |\nabla(W_o - W)|} \tag{11}$$

where $\nabla(W_o - W)$ is the gradient of imbalance, pointing to the most intense area of adsorption reaction. Parameter α represents the synergy effect between the heat transfer and the adsorption reaction driving force, while β represents the synergy effect between the flow and adsorption reaction driving force.

As presented in Fig. 4, α and β reflect the synergy angle between (∇T, $\nabla(W_o - W)$) and (∇P, $\nabla(W_o - W)$), respectively. Based on the Fourier law, the direction of ∇T is opposite to the direction of heat transfer, while the LDF model demonstrates $\nabla(W_o - W)$ as a reflection of adsorption driving force, which always points at the area where adsorption is the most needed. In the adsorption process, discharge of adsorption heat is beneficial to the reaction, which makes the direction of heat transfer favorite to disobey the direction of adsorption driving force. It illustrates that the larger the angle between heat transfer and adsorption driving force, the better the system performance. Thus, a smaller α is favorite for adsorption. For parameter β, the direction of ∇P is opposite to the direction of the pressure drop (flow resistance), which is harmful for adsorption. A smaller β leads to a larger angle between pressure drop and adsorption driving force, thus the reaction avoids the route of high flow resistance, resulting in better system performance.

Varying with spatial location and adsorption time, the proposed two angles have a wide range. At the central region of the domain, ∇P and ∇T are nearly perpendicular to the bottom surface up while $\nabla(W_o - W)$ is just the opposite as the bottom area has a larger adsorption driving force, thus the angles are generally 180 at this region. In some regions near the corner, the angles come to 0 as these areas have better synergy between the heat transfer, flow resistance and adsorption kinetics. The impact of two angles on system performance is explored via calculating their volume average and comparing the results under various bed configurations at a constant adsorption time of 300 s.

2.5. Performance indicators

The performance of an adsorption-based system is estimated by two indicators:

$$SCP = \frac{h_{fg} \times \Delta W_{av,ad}}{t_{cycle}} \tag{12}$$

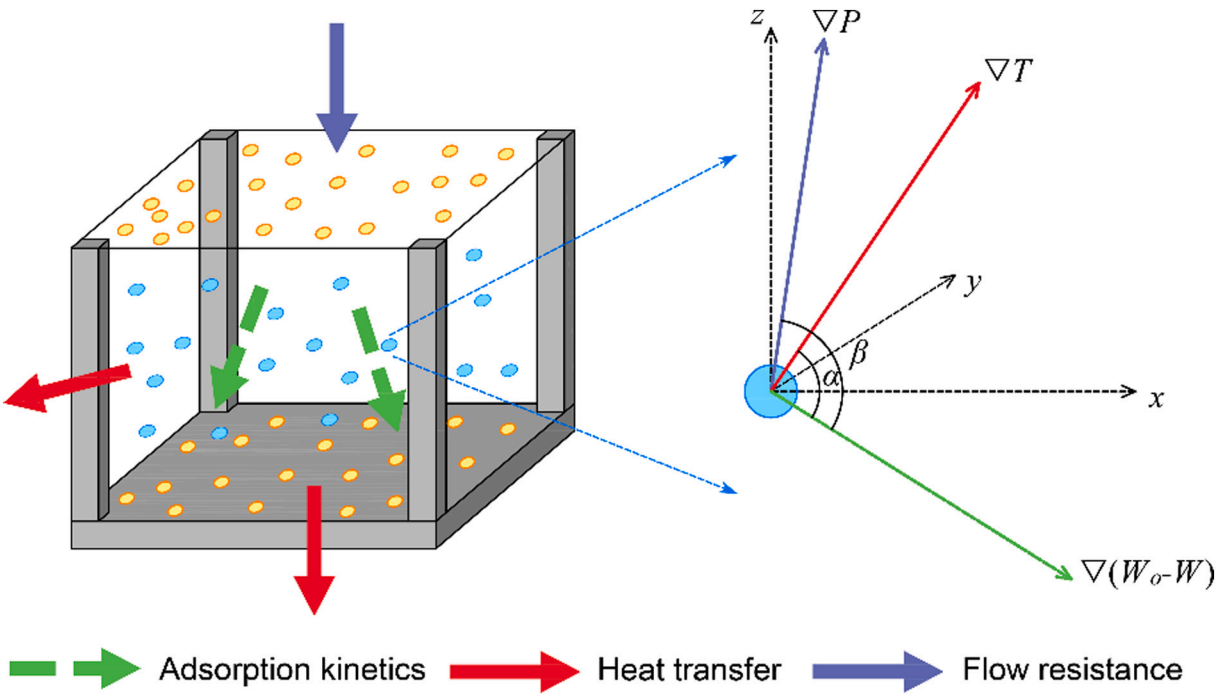

Fig. 4. Schematic of two field synergy parameters employed in the analysis.

$$SDWP = \frac{\Delta W_{av,des}}{\rho_w \times t_{cycle}} \quad (13)$$

where $\Delta W_{av,ad}$ is the volume average of adsorption working capacity, t_{cycle} the cycle time, h_{fg} the latent heat of vaporization under the evaporator pressure. $\Delta W_{av,des}$ is the volume average of desorption working capacity, which is equal to the adsorption working capacity at cyclic steady-state, ρ_w the water density under the condenser temperature.

3. Results and discussion

Two different scenarios of fin arrangement (in-line and fork-row) are proposed and fixed with various fin pitch, fin diameter and fin shape, which are presented in Table 2. We start with a basic field synergy analysis to obtain some relatives between this parameter and the comparatively complicated heat and mass transfer process, thus revealing its effect on the whole system performance. Subsequently, an exploration of the effect of bed configurations on adsorbent performance indicators in terms of average temperature, average uptake, SCP and SDWP is conducted based on the field synergy analysis. Finally, considering different adsorbent mass arising from various bed configurations, an investigation from a bed perspective is conducted to compare the system performances with bed bulk kept constant.

3.1. Grid dependence validation

As shown in Table 5, the grid dependence validation is conducted via a comparison of average temperature and average uptake with different grid sizes and time step configurations. The mesh size on cross-section is manipulated using the built-in control in COMSOL while the direction of bed height is constantly divided. In the simulation, a fork-row fin arrangement is selected with fin pitch and fin diameter fixed at 5 mm and 1 mm respectively. The results presented in Table 5 demonstrated that with a mesh size of 4662 and time step of 1.0 s, the numerical results are accurate enough.

3.2. Adsorbent consideration

3.2.1. The effect of fin diameter

Fig. 5(a) and (b) depict the variations of average temperature and average uptake with the adsorption time for different bed configurations where the fin pitch is fixed at 10 mm while three fin diameters and two fin arrangements are selected. It is evident that for constant fin pitch, decreasing fin diameter causes a lift of bed temperature and a drop of uptake. This is due to the fact that the heat contact surface increases with a larger fin diameter, which decreases the bed temperature and promotes the discharge of adsorption heat, thus leading to an increase in adsorption uptake. On the other hand, it can be observed from Fig. 5(a) that all the bed with the same fin diameter and fork-row fin arrangement possesses a lower average temperature, which manifests its better heat transfer performance. Although the in-line arrangement and fork-row arrangement have the same fin pitch, for a certain amount of adsorbent, the fork-row arrangement comparatively has a larger cooling surface as it has a more compact triangular structure. The augment of cooling surface leads to an elevation of heat transfer performance, which promotes the liberate of adsorption heat and decreases the bed temperature, thus increasing the adsorption uptake, as presented in Fig. 5(b).

In order to generalize the research to a more general situation, a standardization of fin pitch and fin diameter is conducted to use the fin pitch and fin diameter ratio (FP/FD) as an alternative quantity. As presented in Fig. 6, the variation of system performances in terms of specific cooling power and specific daily water production with FP/FD is examined. It can be observed that SCP and SDWP decrease monotonously with the augment of FP/FD, which arises due to the fact that decreasing of fin diameter facilitates the heat transfer process, thus the adsorption uptake. Based on Eqs. (12) and (13), SCP and SDWP vary linearly with the adsorption working capacity, consequently, the cooling effect and fresh water throughput decrease as FP/FD increases. On the other hand, an analysis in field synergy perspective is conducted and the curves of field synergy parameters α and β variations with FP/FD are presented in Fig. 7(a) and (b). As mentioned prior, a worse synergy of heat transfer factor as well as pressure drop factor with the driving force factor (i.e. smaller α and β) is beneficial to the adsorption process. Field synergy results presented in Fig. 7(a) and (b) demonstrate this deduction, as both the parameters α and β augment with larger FP/FD, while SCP and SDWP monotonously decrease. Moreover, beds with a fork-row fin arrangement perform better than the in-line arrangement. For the fin diameter of 6 mm, the system with fork-row arrangement obtains an optimal performance, which is capable of producing 0.397 kW/kg of cooling and 13.6 m^3 per ton silica gel per day of fresh water. As depicted in Fig. 7, the bed with a fork-row arrangement possesses lower α which is favorable to the adsorption process, while the parameter β is approximately the same. This discrepancy may arise due to the fact that the bed aspect ratio, which predominantly impacts the flow resistance, varies a little while the fin arrangement changes. For a proper fin pitch of 10 mm, the little change of aspect ratio brought by the variation of fin arrangements slightly impacts the synergy angle between pressure drop and adsorption driving force, as presented in Fig. 7b. It should be noted that fork-row and in-line arrangements have different angle α at all fin pitches, which arises due to their unequal efficient heat conductivity.

3.2.2. The effect of fin pitch

In this study, three different fin pitches (5 mm, 10 mm, 20 mm) and in-line and fork-row fin arrangements are fixed with the same fin diameter of 2 mm. The variations of average temperature and uptake with the adsorption time are presented in Fig. 8(a) and (b). For a certain amount of adsorbent, a larger fin pitch causes a drop of average heat transfer surface and facilitates the discharge of adsorption heat, thus elevating the bed average temperature, as shown in Fig. 8(a). The higher bed temperature leads to the decreasing of uptake, as presented in Fig. 8 (b). For the proposed two different fin arrangements, a similar conclusion can be derived from this figure. The fork-row arrangement has a lower bed temperature and larger adsorption uptake at various fin pitches.

In Fig. 9(a) and (b), the variations of cooling effect and water throughput with FP/FD for fin pitches of 5 mm, 10 mm, 20 mm and fin arrangements of in-line and fork-row are presented. It can be observed that smaller fin pitch and fork-row arrangement simultaneously lead to a higher SCP and SDWP. For the bed with a fin pitch of 5 mm, fin diameter of 3 mm and fork-row arrangement, the system results in an optimal SCP of 0.407 kW/kg and SDWP of 14.0 m^3/ton silica gel per day. For the fin

Table 5
Effect of grid points and time step on numerical results.

Time step	0.5 s						1.0 s					
Mesh size	2016		4662		6750		2016		4662		6750	
Time	X_{av}	T_{av}	X_{av}	T_{av}	X_{av}	T_{av}	X_{av}	T_{av}	X_{av}	T_{av}	X_{av}	T_{av}
100	0.1175	314.37	0.1174	314.41	0.1173	314.43	0.1175	314.37	0.1174	314.41	0.1173	314.43
300	0.1756	306.76	0.1754	306.79	0.1753	306.80	0.1756	306.76	0.1754	306.79	0.1753	306.80
500	0.2089	303.40	0.2087	303.43	0.2086	303.44	0.2089	303.40	0.2087	303.43	0.2086	303.44

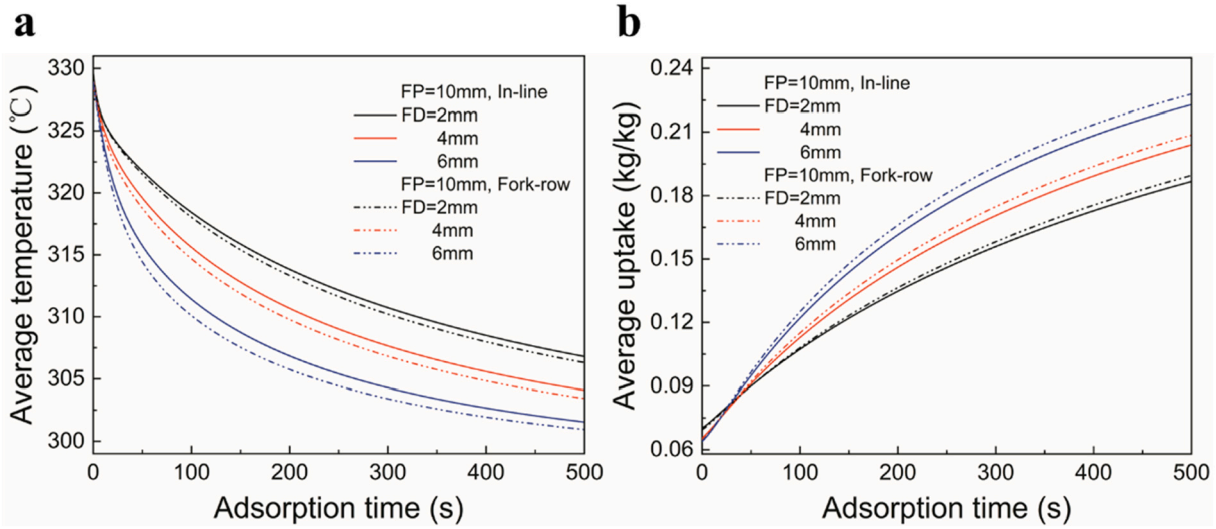

Fig. 5. Variations of (a) average temperature; and (b) average uptake with the adsorption time for different fin diameter and fin arrangement. In the simulation, the fin pitch is fixed at 10 mm.

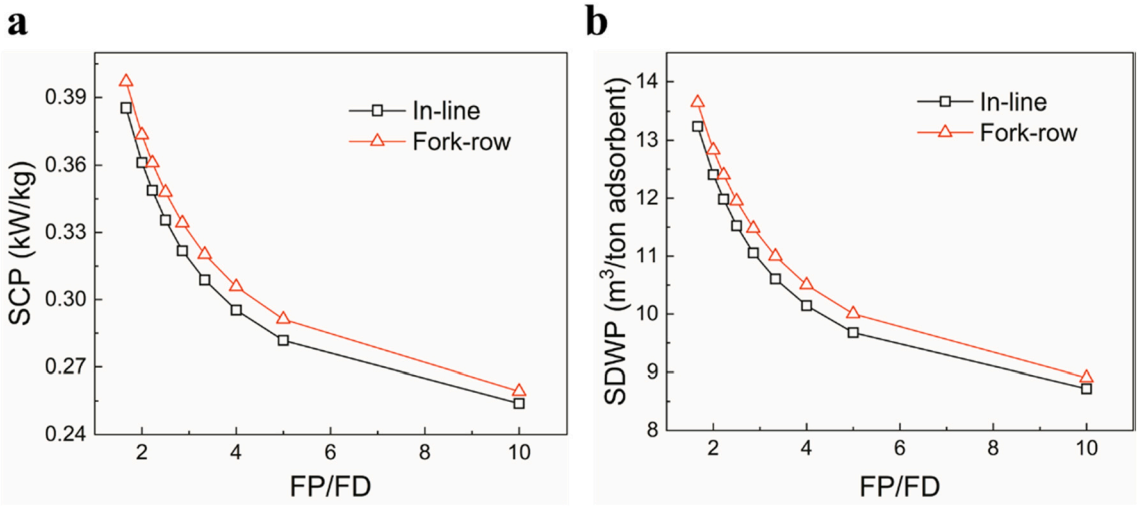

Fig. 6. Variations of (a) SCP; and (b) SDWP with the fin pitch and fin diameter ratio (FP/FD) for different fin arrangement.

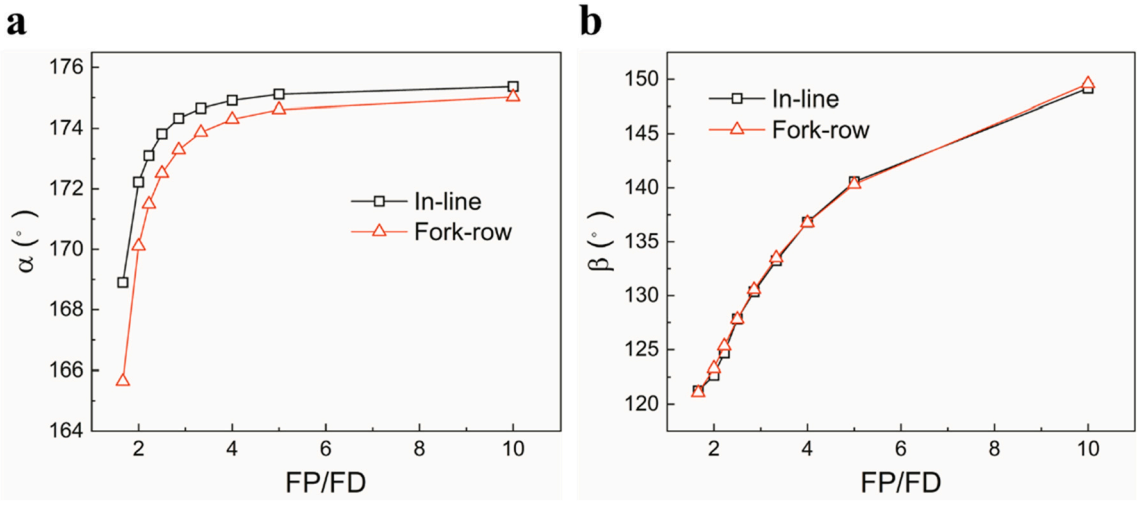

Fig. 7. Variations of field synergy parameters (a) α; and (b) β with the fin pitch and fin diameter ratio (FP/FD) for different fin arrangement.

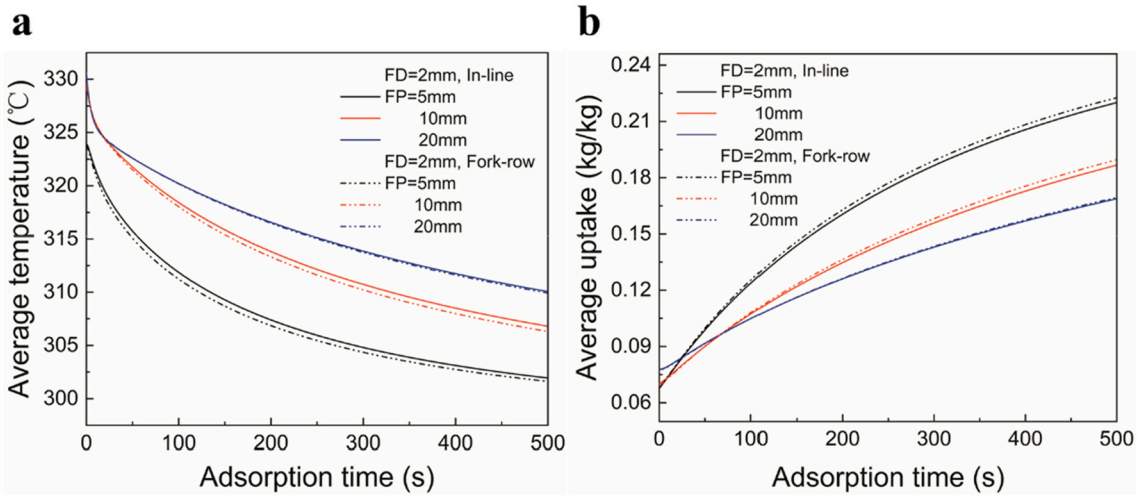

Fig. 8. Variations of (a) average temperature; and (b) average uptake with the adsorption time for different fin pitch and fin arrangement. In the simulation, the fin diameter is fixed at 2 mm.

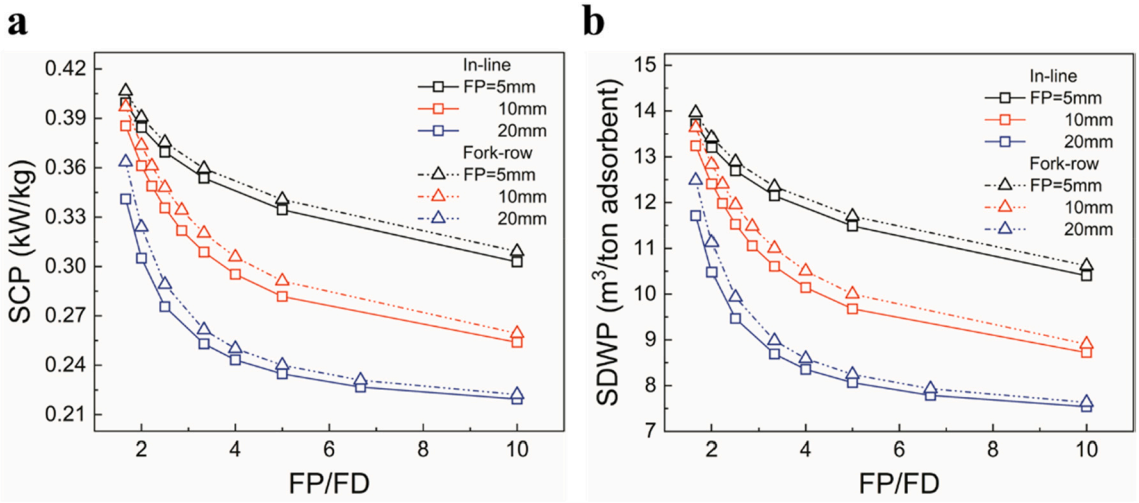

Fig. 9. Variations of (a) SCP; and (b) SDWP with the fin pitch and fin diameter ratio (FP/FD) for different fin pitch and fin arrangement.

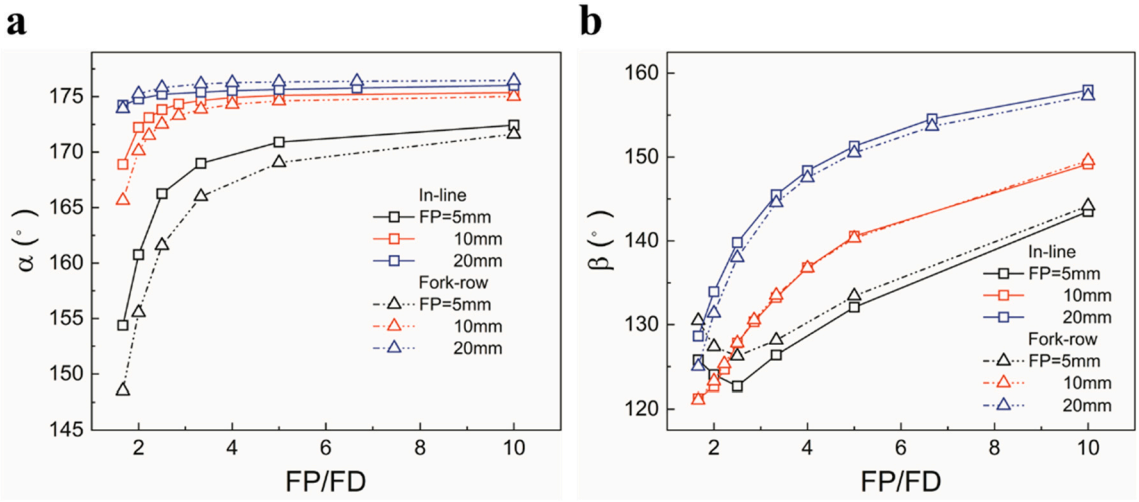

Fig. 10. Variations of field synergy parameters (a) α; and (b) β with the fin pitch and fin diameter ratio (FP/FD) for different fin pitch and fin arrangement.

pitch of 20 mm, fin diameter of 12 mm, the system with fork-row arrangement results in a SCP of 0.363 kW/kg and SDWP of 12.5 m^3 per ton silica gel per day, which is 6.6% higher than that of the in-line arrangement, which is capable of producing 0.341 kW/kg of cooling and 11.7 m^3 per ton silica gel per day of potable water.

As presented in Fig. 10, field parameter α increases as FP/FD augments while the system performances in terms of SCP and SDWP decreases, which still matches the conclusions drawn from Section 2.4. For the field parameter β, the bed with a fin pitch of 10 mm and 20 mm has a similar behavior as Section 3.1 describes. Nevertheless, for the fin pitch of 5 mm, some anomalies present. The angle β reaches the minimum at an approximate FP/FD of 2.5 below which the parameter β decreases as FP/FD increases, still the bed performance deteriorates. This may arise due to the harmful influence of large augment of parameter α in this FP/FD interval, which preponderates the beneficial effect brought by the drop of β. The discrepancy of β may arise because of the sharply increasing flow resistance when a small fin pitch is fixed with a large fin diameter. As for the two fin arrangements, although generally the fork-row performs better in SCP and SDWP, for the fin pitch of 5 mm, the fork-row arrangement has a lower parameter α and larger parameter β while the situation is just the opposite at a fin pitch of 20 mm. It illustrates that the field synergy parameter between heat transfer and the driving force factor is more predominant at a relatively smaller fin pitch, which can also be demonstrated from the prior analysis. Consequently, although the fork-row arrangement possesses a higher β for the fin pitch of 5 mm, it still performs better than the in-line arrangement. There is a similar statement for the fin pitch of 20 mm. At a fin pitch of 10 mm, as the fork-row arrangement has a lower α and similar β compared with the in-line, the two arrangements have the largest deviation.

3.2.3. The effect of fin shape

Three different fin shapes (rectangular, rhombus, circle) are selected to examine their effect on the system performances and the field synergy parameters. To keep the adsorbent mass constant, fins with various fin shapes have the same cross-sectional area. As presented in Fig. 11(a) and (b), the cooling effect and potable water throughput vary a little with different fin shapes. Beds with rectangular fins and rhombus fins perform nearly the same, while bed with circle fins results in a slightly lower SCP and SDWP. This arises due to the shortest perimeter of a circle cross-section possessing the same area with the corresponding rectangular and rhombus cross-sections, thus the smallest side area, which is just the heat exchange area in this finned-flat adsorption bed. Fig. 12 depicts the variations of field synergy parameters α and β at different fin shapes. It can be observed from the figure that the three fin shapes

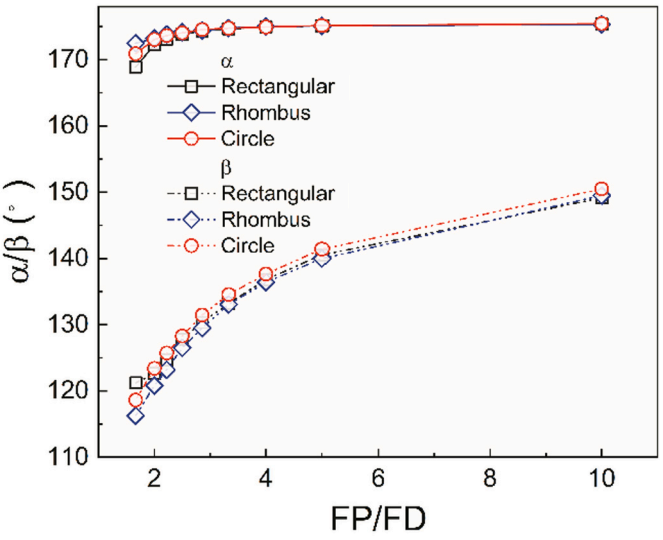

Fig. 12. Variations of field synergy parameters α and β with the fin pitch and fin diameter ratio (FP/FD) for different fin shape. In the simulation, the fin pitch is fixed at 10 mm and the bed has fork-row fin arrangement.

behave nearly the same in terms of α and β, except for the slight elevation of β for the bed with a circle fin shape, which causes its comparatively lower performance.

3.3. Bed consideration

Although increasing the fin diameter can effectively augment the heat exchange surface and enhance the adsorbent performances in terms of SCP and SDWP, as the increase of metal volume causes a lower adsorbent mass for the same bed bulk, the whole system performance may behave differently with the aforementioned investigation. In this part, different fin pitches, fin diameters and fin arrangements are fixed at the same bed bottom area to keep them with an invariant bed volume. The system performances in terms of total cooling power and total daily water production (TDWP) are investigated in Fig. 13(a) and (b). It can be observed from the figure that there is an optimal TCP and TDWP for various FP/FD at each fin pitch. The optimal cooling effect and water production increase with shorter fin pitches and fork-row fin arrangement. For the fin pitch of 5 mm and fin diameter of 1 mm, the bed with fork-row arrangement results in the highest TCP of 6.74×10^{-4} kW and

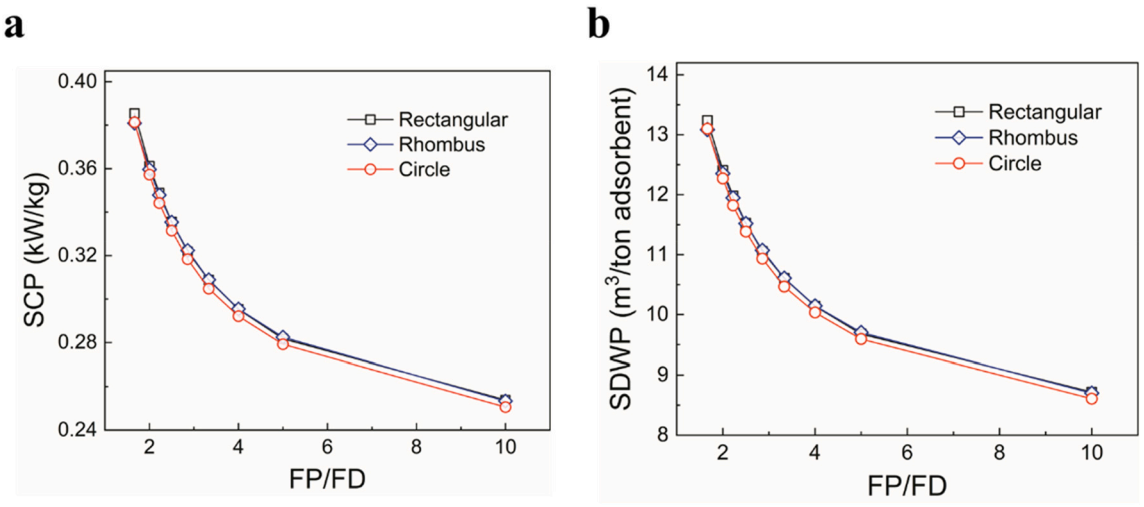

Fig. 11. Variations of (a) SCP; and (b) SDWP with the fin pitch and fin diameter ratio (FP/FD) for different fin shape. In the simulation, the fin pitch is fixed at 10 mm and the bed has fork-row fin arrangement.

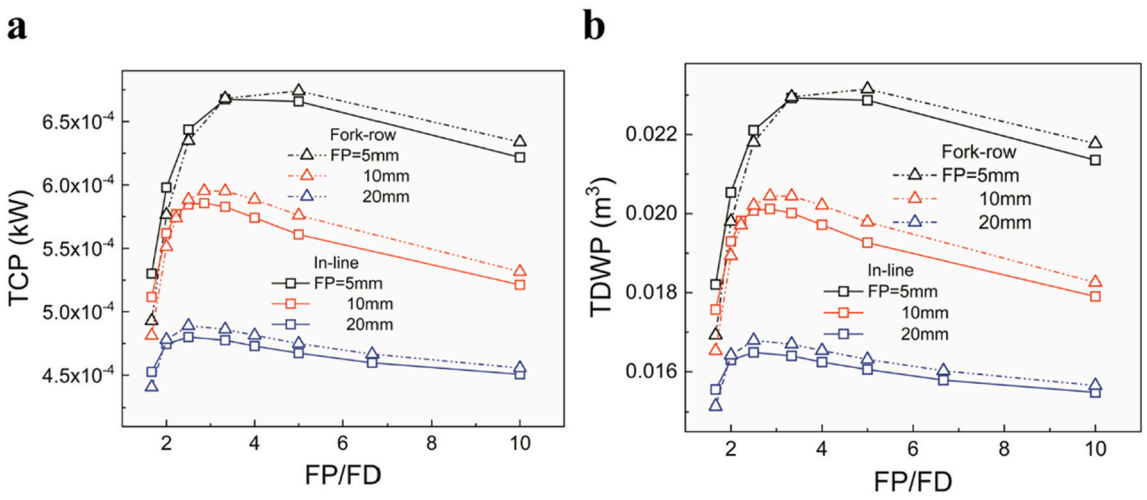

Fig. 13. Variations of (a) TCP; and (b) TDWP with the fin pitch and fin diameter ratio (FP/FD) for different fin pitch and fin arrangement.

SDWP of 0.0232m^3 per day. It should be noted that the derived optimal bed configuration is different from the conclusion drawn in Section 3.3, the investigation in an adsorbent perspective, which gains an optimal bed configuration of the fin pitch of 5 mm, fin diameter of 3 mm, fork-row arrangement. The rapid drop of adsorbent mass caused by the increase of fin diameter results in this deviation. Moreover, the TCP and TDWP of fork-row arrangement is higher than that of the in-line arrangement only at a relatively higher FP/FD, for small FP/FD, the former performs worse than the latter. This may arise due to a lower adsorbent mass of the fork-row arrangement at smaller FP/FD as it has a more compact triangular fin structure.

Based on the aforementioned parametric analysis, a brief study to design a finned-flat bed with proper fin pitch and fin diameter is conducted considering an elevation of TCP and a reduction of bed volume. At a bed height of 12 mm and particle diameter of 0.35 mm, the rectangular fin is selected as the circle fin performs worse in terms of SCP and TCP. Furthermore, for FP/FD larger than 2, the fork-row arrangement results in a higher TCP while the in-line arrangement is a better choice when the ratio reduces to less than 2, as it accompanies with unfavorable deteriorating of TCP. In a modular bed, the decreasing of TCP results in the augment of module number and bed volume, which is harmful to the system's commercialization. Consequently, fork-row arrangement with a shorter fin pitch such as 5 mm and a proper FP/FD within 3 to 4 is favorable for efficiently producing water and cooling.

4. Conclusions

Inserting metal fins inside the adsorbent bed can further compensate for the high heat transfer resistance arising from the loose adsorbent particle, thus advancing the system performance. A modular bed with columnar fins is considered employing a dynamical three-dimensional computational fluid dynamics model along with Darcy's law and LDF model. Field synergy analysis is conducted in this system and two representative angles α and β are selected to reflect the synergy between temperature, pressure and the uptake field. Subsequently, their impacts on heat transfer, flow resistance and the adsorption kinetics thus the system performance are explored with the variation of fin parameters. General findings with respect to field synergy analysis and performance optimization are listed below:

- Angles α and β reflecting the synergy characteristics between heat transfer, flow resistance and the adsorption kinetics should be minimized during the adsorption process.
- The increase of fin diameter (FP/FD decreases) promotes the heat transfer within the bed thus elevating the uptake and SCP.
- At a shorter fin pitch, the fork-row arrangement exhibits a lower parameter α and larger parameter β, resulting in better performance of the fork-row configuration.
- The changes of fin shape slightly impact SCP and the two field synergy angles. Circle fins present worse performance.

CRediT authorship contribution statement

Mingliang Li: Writing – Original draft. **Yanan Zhao**: Visualization. **Rui Long**: Conceptualization, Writing – Review & Editing. **Zhichun Liu**: Investigation. **Wei Liu**: Formal analysis.

Declaration of competing interest

The authors declare no competing financial interest.

Acknowledgements

This work was financially supported by the National Natural Science Foundation of China (51736004).

References

[1] B.B. Saha, I.I. El-Sharkawy, M.W. Shahzad, K. Thu, L. Ang, K.C. Ng, Fundamental and application aspects of adsorption cooling and desalination, Appl. Therm. Eng. 97 (2016) 68–76.
[2] K.C. Ng, K. Thu, S.J. Oh, L. Ang, M.W. Shahzad, A.B. Ismail, Recent developments in thermally-driven seawater desalination: energy efficiency improvement by hybridization of the MED and AD cycles, Desalination 356 (2015) 255–270.
[3] S. Lin, H. Zhao, L. Zhu, T. He, S. Chen, C. Gao, et al., Seawater desalination technology and engineering in China: a review, Desalination 498 (2021), 114728.
[4] M. Li, Y. Zhao, R. Long, Z. Liu, W. Liu, Gradient porosity distribution of adsorbent bed for efficient adsorption cooling, Int. J. Refrig. 128 (2021) 153–162.
[5] J.W. Wu, E.J. Hu, M.J. Biggs, Thermodynamic cycles of adsorption desalination system, Appl. Energy 90 (1) (2012) 316–322.
[6] R. Long, Y. Zhao, M. Li, Y. Pan, Z. Liu, W. Liu, Evaluations of adsorbents and salt-methanol solutions for low-grade heat driven osmotic heat engines, Energy 229 (2021), 120798.
[7] K. Thu, B.B. Saha, K.J. Chua, K.C. Ng, Performance investigation of a waste heat-driven 3-bed 2-evaporator adsorption cycle for cooling and desalination, Int. J. Heat Mass Transf. 101 (2016) 1111–1122.
[8] A.S. Alsaman, A.A. Askalany, K. Harby, M.S. Ahmed, Performance evaluation of a solar-driven adsorption desalination-cooling system, Energy 128 (2017) 196–207.
[9] F.N. Al-Mousawi, R. Al-Dadah, S. Mahmoud, Novel system for cooling and electricity: four different integrated adsorption-ORC configurations with two expanders, Energy Convers. Manag. 152 (2017) 72–87.
[10] Y. Zhao, M. Li, R. Long, Z. Liu, W. Liu, Dynamic modelling and analysis of an adsorption-based power and cooling cogeneration system, Energ. Convers. Manage. 222 (2020), 113229.
[11] Y. Zhao, Z. Luo, R. Long, Z. Liu, W. Liu, Performance evaluations of an adsorption-based power and cooling cogeneration system under different operative conditions and working fluids, Energy 204 (2020), 117993.

[12] R. Long, X. Xia, Y. Zhao, S. Li, Z. Liu, W. Liu, Screening metal-organic frameworks for adsorption-driven osmotic heat engines via grand canonical Monte Carlo simulations and machine learning, iScience 24 (1) (2021) 101914.
[13] M. Ghazy, A.A. Askalany, K. Harby, M.S. Ahmed, Adsorption isotherms and kinetics of HFC-404A onto bituminous based granular activated carbon for storage and cooling applications, Appl. Therm. Eng. 105 (2016) 639–645.
[14] J.W. Wu, M.J. Biggs, P. Pendleton, A. Badalyan, E.J. Hu, Experimental implementation and validation of thermodynamic cycles of adsorption-based desalination, Appl. Energy 98 (2012) 190–197.
[15] E. Elsayed, R. Al-Dadah, S. Mahmoud, P. Anderson, A. Elsayed, Adsorption cooling system employing novel MIL-101(Cr)/CaCl2 composites: numerical study, Int. J. Refrig. 107 (2019) 246–261.
[16] E. Elsayed, R. Al-Dadah, S. Mahmoud, P.A. Anderson, A. Elsayed, P.G. Youssef, CPO-27(Ni), aluminium fumarate and MIL-101(Cr) MOF materials for adsorption water desalination, Desalination 406 (2017) 25–36.
[17] H.W.B. Teo, A. Chakraborty, Y. Kitagawa, S. Kayal, Experimental study of isotherms and kinetics for adsorption of water on aluminium fumarate, Int. J. Heat Mass Transf. 114 (2017) 621–627.
[18] E. Elsayed, R. Al-Dadah, S. Mahmoud, A. Elsayed, P.A. Anderson, Aluminium fumarate and CPO-27(Ni) MOFs: characterization and thermodynamic analysis for adsorption heat pump applications, Appl. Therm. Eng. 99 (2016) 802–812.
[19] M. Mahdavikhah, H. Niazmand, Effects of plate finned heat exchanger parameters on the adsorption chiller performance, Appl. Therm. Eng. 50 (1) (2013) 939–949.
[20] S. Mitra, P. Kumar, K. Srinivasan, P. Dutta, Performance evaluation of a two-stage silica gel + water adsorption based cooling-cum-desalination system, Int. J. Refrig. 58 (2015) 186–198.
[21] S.M. Ali, A. Chakraborty, Adsorption assisted double stage cooling and desalination employing silica gel + water and AQSOA-Z02 + water systems, Energy Convers. Manag. 117 (2016) 193–205.
[22] P.G. Youssef, S.M. Mahmoud, R.K. Al-Dadah, Performance analysis of four bed adsorption water desalination/refrigeration system, comparison of AQSOA-Z02 to silica-gel, Desalination 375 (2015) 100–107.
[23] P.G. Youssef, S.M. Mahmoud, R.K. Al-Dadah, Numerical simulation of combined adsorption desalination and cooling cycles with integrated evaporator/condenser, Desalination 392 (2016) 14–24.
[24] K. Thu, A. Chakraborty, Y.-D. Kim, A. Myat, B.B. Saha, K.C. Ng, Numerical simulation and performance investigation of an advanced adsorption desalination cycle, Desalination 308 (2013) 209–218.
[25] K. Thu, B.B. Saha, A. Chakraborty, W.G. Chun, K.C. Ng, Study on an advanced adsorption desalination cycle with evaporator–condenser heat recovery circuit, Int. J. Heat Mass Transf. 54 (1–3) (2011) 43–51.
[26] M.M. Abd-Elhady, A.M. Hamed, Effect of fin design parameters on the performance of a two-bed adsorption chiller, Int. J. Refrig. 113 (2020) 164–173.
[27] T. Miyazaki, A. Akisawa, B.B. Saha, I.I. El-Sharkawy, A. Chakraborty, A new cycle time allocation for enhancing the performance of two-bed adsorption chillers, Int. J. Refrig. 32 (5) (2009) 846–853.
[28] I.S. Glaznev, Y.I. Aristov, The effect of cycle boundary conditions and adsorbent grain size on the water sorption dynamics in adsorption chillers, Int. J. Heat Mass Transf. 53 (9–10) (2010) 1893–1898.
[29] A. Chakraborty, B.B. Saha, Y.I. Aristov, Dynamic behaviors of adsorption chiller: effects of the silica gel grain size and layers, Energy 78 (2014) 304–312.
[30] A. Freni, G. Maggio, F. Cipitì, Y.I. Aristov, Simulation of water sorption dynamics in adsorption chillers: one, two and four layers of loose silica grains, Appl. Therm. Eng. 44 (2012) 69–77.
[31] Y.I. Aristov, Experimental and numerical study of adsorptive chiller dynamics: loose grains configuration, Appl. Therm. Eng. 61 (2) (2013) 841–847.
[32] R.H. Mohammed, O. Mesalhy, M.L. Elsayed, L.C. Chow, Assessment of numerical models in the evaluation of adsorption cooling system performance, Int. J. Refrig. 99 (2019) 166–175.
[33] Y.I. Aristov, B. Dawoud, I.S. Glaznev, A. Elyas, A new methodology of studying the dynamics of water sorption/desorption under real operating conditions of adsorption heat pumps: experiment, Int. J. Heat Mass Transf. 51 (19–20) (2008) 4966–4972.
[34] Y.I. Aristov, M.M. Tokarev, A. Freni, I.S. Glaznev, G. Restuccia, Kinetics of water adsorption on silica Fuji Davison RD, Microporous Mesoporous Mater. 96 (1–3) (2006) 65–71.
[35] S. Jribi, T. Miyazaki, B.B. Saha, S. Koyama, S. Maeda, T. Maruyama, Corrected adsorption rate model of activated carbon–ethanol pair by means of CFD simulation, Int. J. Refrig. 71 (2016) 60–68.
[36] S. Mitra, M. Muttakin, K. Thu, B.B. Saha, Study on the influence of adsorbent particle size and heat exchanger aspect ratio on dynamic adsorption characteristics, Appl. Therm. Eng. 133 (2018) 764–773.
[37] S. Mitra, N. Aswin, P. Dutta, Scaling analysis and numerical studies on water vapour adsorption in a columnar porous silica gel bed, Int. J. Heat Mass Transf. 95 (2016) 853–864.
[38] M.M. Saleh, R. Al-Dadah, S. Mahmoud, E. Elsayed, O. El-Samni, Wire fin heat exchanger using aluminium fumarate for adsorption heat pumps, Appl. Therm. Eng. 164 (2020).
[39] H. Niazmand, I. Dabzadeh, Numerical simulation of heat and mass transfer in adsorbent beds with annular fins, Int. J. Refrig. 35 (3) (2012) 581–593.
[40] M. Mohammadzadeh Kowsari, H. Niazmand, M.M. Tokarev, Bed configuration effects on the finned flat-tube adsorption heat exchanger performance: numerical modeling and experimental validation, Appl. Energy 213 (2018) 540–554.
[41] M. Li, Y. Zhao, R. Long, Z. Liu, W. Liu, Computational fluid dynamic study on adsorption-based desalination and cooling systems with stepwise porosity distribution, Desalination 508 (2021).
[42] R.H. Mohammed, O. Mesalhy, M.L. Elsayed, L.C. Chow, Performance evaluation of a new modular packed bed for adsorption cooling systems, Appl. Therm. Eng. 136 (2018) 293–300.
[43] J.W. Wu, M.J. Biggs, E.J. Hu, Dynamic model for the optimisation of adsorption-based desalination processes, Appl. Therm. Eng. 66 (1–2) (2014) 464–473.
[44] R.H. Mohammed, O. Mesalhy, M.L. Elsayed, L.C. Chow, Scaling analysis of heat and mass transfer processes in an adsorption packed bed, Int. J. Therm. Sci. 133 (2018) 82–89.
[45] I.I. El-Sharkawy, On the linear driving force approximation for adsorption cooling applications, Int. J. Refrig. 34 (3) (2011) 667–673.
[46] R.H. Mohammed, O. Mesalhy, M.L. Elsayed, M. Su, C. Chow L., Revisiting the adsorption equilibrium equations of silica-gel/water for adsorption cooling applications, Int. J. Refrig. 86 (2018) 40–47.
[47] K. Thu, A. Chakraborty, B.B. Saha, K.C. Ng, Thermo-physical properties of silica gel for adsorption desalination cycle, Appl. Therm. Eng. 50 (2) (2013) 1596–1602.
[48] I. Solmus, S. Andrew, D. Rees, C. Yamali, D. Baker, A two-energy equation model for dynamic heat and mass transfer in an adsorbent bed using silica gel/water pair, Int. J. Heat Mass Transf. 55 (19–20) (2012) 5275–5288.
[49] R.H. Mohammed, A simplified method for modeling of round and square ceiling diffusers, Energ. Buildings 64 (2013) 473–482.
[50] M.A. Aziz, I.A.M. Gad, E.S.F.A. Mohammed, R.H. Mohammed, Experimental and numerical study of influence of air ceiling diffusers on room air flow characteristics, Energ. Buildings 55 (2012) 738–746.
[51] D. Cheng, E.A.J.F. Peters, J.A.M. Kuipers, Performance study of heat and mass transfer in an adsorption process by numerical simulation, Chem. Eng. Sci. 160 (2017) 335–345.
[52] F.N. Al-Mousawi, R. Al-Dadah, S. Mahmoud, Different bed configurations and time ratios: performance analysis of low-grade heat driven adsorption system for cooling and electricity, Energy Convers. Manag. 148 (2017) 1028–1040.
[53] H.T. El-Dessouky, HME. Fundamentals of Salt Water Desalination, Elsevier Science B V, 2020.